Engineering the Hydrophobic Pocket of Carbonic Anhydrase II[†,‡]

Richard S. Alexander, Satish K. Nair, and David W. Christianson*

Department of Chemistry, University of Pennsylvania, Philadelphia, Pennsylvania 19104-6323

Received May 31, 1991; Revised Manuscript Received August 26, 1991

ABSTRACT: Wild-type and mutant human carbonic anhydrases II, where mutations have been made in the hydrophobic pocket of the active site, have been studied by X-ray crystallographic methods. Specifically, mutations at Val-143 (the base of the pocket) lead to significant changes in catalytic activity and protein structure. The obliteration of a well-defined pocket in the Val-143 → Phe and Val-143 → Tyr mutants results in significantly diminished enzyme activity [(5×10^4)-fold and (3×10^5)-fold, respectively]; however, the activity of the Val-143 → His mutant is diminished less (10^2-fold), and deepening the pocket in the Val-143 → Gly mutant results in only a 2-fold decrease in activity [Fierke et al., 1991 (preceding paper in this issue)]. These results indicate that the hydrophobic pocket is important for substrate association with the enzyme, but there are probably several catalytically acceptable substrate trajectories through this region of the enzyme structure. Additionally, each mutant protein exhibits long-range (ca. 10–15 Å) compensatory structural changes which accommodate the Val-143 substitution. As such, the genetic–structural approach represented in this work serves as a three-dimensional paradigm for the redesign of specificity pockets in other protein catalysts.

Human carbonic anhydrase II (CAII;[1] EC 4.2.1.1) is a metalloenzyme containing one catalytically required zinc ion bound to a single polypeptide chain of 260 amino acids [for recent reviews, see Coleman (1986), Lindskog (1986), Silverman and Lindskog (1988), and Christianson (1991)]. In the erythrocyte, CAII catalyzes the hydration of carbon dioxide into bicarbonate ion plus a proton (Figure 1), exhibiting the second-order rate constant $k_{cat}/K_M = 1.5 \times 10^8$ M^{-1} s^{-1}. These kinetics are comparable to those of a diffusion control reaction and distinguish CAII from other known isozymes (Lindskog, 1983, 1986; Silverman & Lindskog, 1988). However, since the product proton must be transferred to bulk solvent, the participation of buffer is necessary in order to achieve the measured turnover rate of 10^6 s^{-1} (Eigen & Hammes, 1963; Silverman & Tu, 1975; Jonsson et al., 1976).

The structure of carbonic anhydrase II from human blood has been determined (Liljas et al., 1972) and refined at 2.0-Å resolution (Eriksson et al., 1986, 1988a). The enzyme is roughly spherical and the active site comprises a conical cleft about 15 Å deep. The zinc ion lies at the bottom of this cleft and is tetrahedrally liganded by His-94, His-96, His-119, and hydroxide ion at physiological pH. Important polar residues in the active site include Thr-199, which accepts a hydrogen bond from zinc-bound hydroxide and donates a hydrogen bond to Glu-106 (Eriksson et al., 1986, 1988a), and His-64, which serves as a proton shuttle in the conversion of zinc-bound water into zinc-bound hydroxide (Steiner et al., 1975; Liang & Lipscomb, 1988; Tu et al., 1989). Zinc-bound hydroxide is the nucleophile which attacks substrate CO_2 in the catalytic mechanism (Coleman, 1967; Lindskog & Coleman, 1973).

About half of the active-site cleft of CAII is hydrophobic in nature, and there is a noticeable pocket in this region, largely defined by Trp-209, Val-121, Leu-198, and Val-143, adjacent to the zinc-bound hydroxide group. Although the catalytic role of nonpolar residues in the CAII active site is not clear, those residues comprising the hydrophobic pocket are believed to be important for enzyme–substrate association. In native CAII, the so-called "deep" water molecule is located at the mouth of the pocket and makes van der Waals contacts with pocket residues Leu-198 and Trp-209 (Lindskog, 1986; Eriksson et al., 1986, 1988a). This water molecule is displaced upon the binding of certain inhibitors (Eriksson et al., 1986, 1988b), and it is believed that this water is likewise displaced by substrate CO_2 (Lindskog, 1986). Hence, the hydrophobic pocket may be a precatalytic substrate association site. The results of several spectroscopic studies have been interpreted to identify an enzyme–substrate complex where CO_2 does not coordinate to zinc in inner-sphere fashion, and these results are in accord with substrate association in the hydrophobic pocket (Riepe & Wang, 1968; Stein et al., 1977; Bertini et al., 1979, 1983, 1987; Led et al., 1982; Williams & Henkens, 1985). Additionally, recent molecular dynamics simulations of the enzyme–substrate complex indicate that the pocket is a favorable location for CO_2 association (Merz, 1990, 1991; Liang & Lipscomb, 1990). However, it is conceivable that, while CO_2 associates with the enzyme in the region of the hydrophobic pocket, CO_2 may additionally interact with a fifth coordination site on zinc in outer-sphere fashion (Eriksson et al., 1986, 1988b; Merz, 1990; Liang & Lipscomb, 1990).

Here, we report structure–function relationships in the active-site pocket of CAII by X-ray crystallographic analysis of certain site-specific mutant enzymes. In particular, the structures of mutant CAIIs have been determined where Val-143 (located at the base of the hydrophobic pocket) has been substituted by the amino acids Gly (V143G), His (V143H), Phe (V143F), and Tyr (V143Y). Hence, the hydrophobic pocket is made deeper in the V143G mutant,

[†] We thank NSF for Grant DIR-8821184 (in support of the X-ray data acquisition equipment) and the NIH for Grant GM45614. Additionally, D.W.C. is grateful to the Office of Naval Research for a Young Investigator Award and the Chicago Community Trust for a Searle Scholar Award. S.K.N. is supported by NIH Training Grant GM07229.

[‡] Coordinates for wild-type CAII and the mutants V143F, V143G, V143H, and V143Y have been deposited in the Brookhaven Protein Data Bank.

[1] Abbreviations: CAII, human carbonic anhydrase II; wt, wild type; V143Y, Val-143 → Tyr; V143F, Val-143 → Phe; V143H, Val-143 → His; V143G, Val-143 → Gly.

0006-2960/91/0430-11064$02.50/0 © 1991 American Chemical Society

Table I: Data Collection and Refinement Statistics for Wild-Type and Mutant Carbonic Anhydrases II

	wild type	V143Y	V143F	V143H	V143G
no. of crystals	3	2	2	2	2
no. of measured reflections	20760	13723	14169	18465	14191
no. of unique reflections	10200	7413	8571	8367	6772
max resolution (Å)	2.1	2.8	2.5	2.4	2.4
$R_m(F)$[a]	0.092	0.097	0.086	0.085	0.091
no. of water molecules in final cycle of refinement	102	76	83	66	89
no. of reflections used in refinement (6.5 – max resolution, Å)	9346	5037	6755	6990	6298
R factor[b]	0.183	0.183	0.186	0.176	0.176
rms deviation from ideal bond lengths (Å)	0.026	0.004	0.013	0.006	0.016
rms deviation from ideal bond angles (degrees)	1.9	2.1	1.3	2.3	1.3
rms deviation from ideal planarity (Å)	0.012	0.005	0.007	0.007	0.007
rms deviation from ideal chirality (Å^3)	0.140	0.064	0.081	0.076	0.067

[a] R_{merge} for replicate reflections, $R = \sum||F_{hi}| - \langle|F_h|\rangle|/\sum\langle|F_h|\rangle$; $|F_h|$ = scaled structure factor for reflection h in data set i. $\langle|F_h|\rangle$ = average structure factor for reflection h from replicate data. [b] Crystallographic R factor, $R = \sum||F_o| - |F_c||/\sum|F_o|$; $|F_o|$ and $|F_c|$ are the observed and calculated structure factors, respectively.

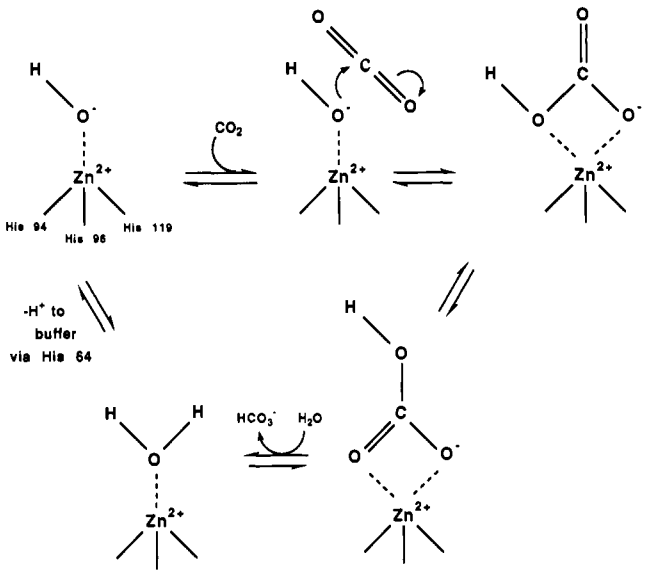

FIGURE 1: Summary of the CO_2 hydrase mechanism catalyzed by human carbonic anhydrase II.

whereas the pocket is made shallower in the V143H, V143F, and V143Y mutants. Kinetic studies of Val-143 mutants [Fierke et al., 1991 (preceding paper in this issue)] interpreted in light of their three-dimensional structures allow for significant mechanistic conclusions regarding the role of the pocket in substrate association and catalysis. Moreover, the current study allows for an evaluation of the structural consequences of modifying the base of an enzyme specificity pocket, and the resulting lessons in protein design will carry over to experiments with other protein catalysts.

Experimental Procedures

Recombinant wild-type, V143G, V143H, V143F, and V143Y CAIIs were generously provided by Professor Carol Fierke, Duke University, and enzyme crystallizations were performed by the sitting-drop method. Typically, a 20-μL drop containing 0.3 mM enzyme, 50 mM Tris-HCl (pH 8.0 at room temperature), 150 mM NaCl, and 3 mM NaN_3 was added to a 20-μL drop containing 50 mM Tris-HCl (pH 8.0 at room temperature), 150 mM NaCl, and 3 mM NaN_3 with 1.75–2.5 M ammonium sulfate in the crystallization well. Both solutions were saturated with methyl mercury acetate in order to facilitate the growth of diffraction-quality parallelepipedons (Tilander et al., 1965). Additionally, the addition of 0.1 mM octyl β-glucoside to the enzyme buffer was critical for the crystallization of certain mutant proteins (McPherson et al., 1986). Crystals of typical dimensions 0.2 mm × 0.2 mm × 0.8 mm appeared within 2 weeks at 4 °C. Wild-type and mutant CAIIs crystallized in space group $P2_1$ and exhibited typical unit cell parameters of a = 42.7 Å, b = 41.7 Å, c = 73.0 Å, and β = 104.6°. Importantly, crystals of the wild-type and mutant proteins were isomorphous with those obtained from the native human enzyme in spite of a small difference at the amino termini: native human CAII has Ac-Ser (Henderson et al., 1976), and recombinant CAIIs have Met-Ala [it is not clear that N-terminal Met has been post-translationally cleaved in this system, although the N-terminal Met in constructs beginning with Met-Ser is shown to be cleaved (Forsman et al., 1988)].

Crystals of wild-type and mutant CAIIs were mounted and sealed in 0.5-mm glass capillaries with a small portion of mother liquor. A Siemens X-100A multiwire area detector, mounted on a three-axis camera and equipped with Charles Supper double X-ray focusing mirrors, was used for X-ray data acquisition. A Rigaku RU-200 rotating anode X-ray generator operating at 45 kV/65 mA supplied Cu Kα radiation. All data were collected at room temperature by the oscillation method; the crystal-to-detector distance was set at 14 cm and the detector swing angle was fixed between 20° and 27° in at least four runs per experiment. Data frames of 0.08–0.10° oscillation about ω were collected, with exposure times of 60 s/frame, for total angular rotation ranges about ω of at least 70° per run. Multiple data sets for wild-type and mutant CAIIs were collected, and diffraction intensities were measured to limiting resolutions of 2.1–2.8 Å; these particular crystalline mutants did not diffract as well as the wild-type protein (Table I). Raw data frames were analyzed using the BUDDHA package (Durbin et al., 1986) and replicate and symmetry-related structure factors were merged using PROTEIN (Steigemann, 1974); final merging R factors for wild-type and mutant CAIIs, as well as other relevant data reduction statistics, are recorded in Table I.

In the analysis of the wild-type CAII crystal structure, structure factors obtained from the corrected intensity data were used to generate difference electron density maps using Fourier coefficients $2|F_o| - |F_c|$ and $|F_o| - |F_c|$ with phases calculated from the structure of refined human CAII (Eriksson et al., 1986, 1988a; atomic coordinates were generously provided by Dr. T. Alwyn Jones). Fast Fourier transform routines were employed in all electron density map and structure factor calculations (Ten Eyck, 1973, 1977). Inspection of the electron density maps revealed that only minor adjustments to the protein model were required, and model building was performed with the graphics software FRODO (Jones, 1985) installed on an Evans and Sutherland PS390 interfaced with a VAXstation 3500. Atomic coordinates were then refined

against the observed data by the reciprocal space least-squares method using the stereochemically restrained least-squares algorithm of Hendrickson and Konnert [1981; also see Hendrickson (1985)]. Active-site water molecules were not included in the initial stages of refinement. Residue conformations throughout the protein were examined during the course of refinement by using maps calculated with Fourier coefficients outlined above and phases derived from the in-progress atomic model. Only minimal adjustments of atomic positions were necessary, and active-site water molecules were added when the crystallographic R factor dropped below 0.200. Refinement converged smoothly to a final crystallographic R factor of 0.183 for wild-type CAII; the final model had excellent stereochemistry with rms deviations from ideal bond lengths and angles of 0.026 Å and 1.9°, respectively. Pertinent refinement statistics are recorded in Table I.

A similar protocol was followed for the analysis of mutant CAIIs, but the refined model of wild-type CAII was used as the starting point. For each mutant CAII structure determination, the Fourier coefficients outlined above were used to generate difference electron density maps, where the atoms of residue 143 were deleted from the model prior to the structure factor calculation. Then, the mutant side chain of residue 143 was built into these maps. For each mutant, inspection of the remainder of the protein structure showed that only minor adjustments to the protein model were required prior to least-squares refinement. As for wild-type CAII, active-site water molecules were not included in the initial stages of refinement for each mutant, and residue conformations throughout each mutant were examined during the course of refinement. Active-site water molecules were added to each structure when the crystallographic R factor dropped below 0.200, and refinements converged smoothly to final crystallographic R factors within the range 0.176–0.183. Each final model had excellent stereochemistry with rms deviations from ideal bond lengths and angles within the ranges 0.004 – 0.026 Å and 1.3 – 2.3°, respectively. Pertinent refinement statistics are recorded in Table I.

For the refined structures of wild-type, V143G, V143H, V143F, and V143Y CAIIs, a difference electron density map calculated with Fourier coefficients $|F_o| - |F_c|$ and phases derived from the coordinates of each final model revealed that the highest peaks in the vicinity of the active site were just under 3.5σ in each structure. The rms error in atomic positions for each structure was estimated to be ca. 0.2 Å on the basis of relationships derived by Luzzati (1952). The coordinates of wild-type and mutant CAIIs have been deposited in the Brookhaven Protein Data Bank (Bernstein et al., 1977), with reference codes as follows: wild-type CAII, 4CA2; V143F CAII, 6CA2; V143G CAII, 7CA2; V143H CAII, 8CA2; V143Y CAII, 9CA2.

Results

Wild-Type Carbonic Anhydrase II. The refined structure of wild-type CAII is very similar to that of the human blood enzyme (Eriksson et al., 1986, 1988a), with the occasional exception of some surface residues. However, surface residues are sometimes characterized by weak or discontinuous peaks in electron density maps and thus experience conformational variation in crystallographic refinement. Least-squares superposition of blood CAII and wild-type CAII Cα coordinates [using the software INSIGHT (Biosym, Inc.)] yields an rms difference of 0.2 Å between the two structures. Given the rms coordinate error of ca. 0.2 Å for wild-type CAII calculated from relationships derived by Luzzati (1952), it is reasonable to conclude that the two structures are essentially identical.

Table II: Torsion Angles for Residue 143[a]

	wt	V143G	V143H	V143F	V143Y
ϕ	−118	−96	−109	−105	−112
ψ	+136	+122	+127	+127	+127
χ_1	−54		−83	−87	−87
χ_2			+42	+67	+51

[a] Given in degrees.

Active-site solvent structure is likewise similar between the two structures, and the so-called "deep" water molecule is still found at the mouth of the hydrophobic pocket in wild-type CAII. However, electron density corresponding to this water in the wild-type protein is in a position 2.8 Å away from its position in the human blood enzyme, and in the hydrophobic pocket it makes van der Waals contacts with Val-121, Val-143, and Leu-198.

A mercury ion (Hg^{2+}) binds to Cys-206 in wild-type CAII (and also in the mutant CAIIs). As discussed under Experimental Procedures, CAII must be crystallized in the presence of methyl mercury acetate in order to facilitate the growth of diffraction-quality parallelepipedons (Tilander et al., 1965). However, it must be emphasized that this is not the inhibitory binding mode of mercury reported at His-64 in crystals stabilized in 20% poly(ethylene glycol) 6000 soaked with $HgCl_2$ under different conditions (Eriksson et al., 1986, 1988b). Additionally, the binding of mercury to Cys-206 does not result in significant structural differences between wild-type Hg^{2+}–CAII and Hg^{2+}-free blood CAII (apart from a conformational change of the Cys-206 side chain), so no attempts were made to dialyze mercury out of CAII crystals prior to X-ray data acquisition.

Although the overall structures of blood CAII and wild-type CAII are essentially identical, a few minor differences are revealed upon close inspection of the refined atomic models. For instance, His-4 is present in the model of the blood enzyme, but no unambiguous electron density is observed for this residue in maps of the recombinant wild-type or mutant enzymes. Another difference involves the side chain of His-64, the catalytic proton shuttle, which moves away slightly from the active site. His-64 exhibits conformational mobility in the Thr-200 → Ser mutant of CAII (105° about χ_1, as compared with wild-type CAII; Krebs et al., 1991), and also in the structure of native blood CAII at pH 5.7 (64° about χ_1, as compared with native blood CAII; Nair & Christianson, 1991). The mobility of His-64 observed in these independent crystallographic studies probably accompanies its role as a catalytic proton shuttle.

Mutant Carbonic Anhydrases II. Apart from the contour of the hydrophobic pocket and occasional surface residues, there are no major structural differences distinguishing mutant CAIIs from the wild-type enzyme. However, there are subtle differences among the five structures which reflect the plastic accommodation of the protein scaffolding to individual point mutations—these differences are discussed in a subsequent section. Here, we discuss the structural differences among the hydrophobic pockets of each mutant CAII, and then we summarize the differences observed in the zinc coordination polyhedra among the mutants.

As expected, the three-dimensional structures of V143F and V143Y CAIIs reveal that the bulky six-membered rings of the aromatic groups fill up the hydrophobic pocket, and each aromatic ring tends toward an imperfect "edge-to-face" interaction (Burley & Petsko, 1988) with Trp-209. The χ_1 values for each aromatic side chain are equal, although the χ_2 values differ by 16° (Table II). Differences in χ_2 values appear to arise from slight disorder as the planar six-membered

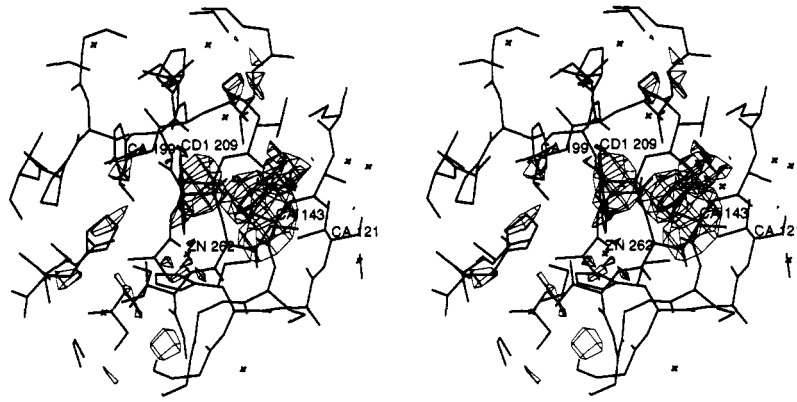

FIGURE 2: Difference electron density map of V143Y CAII, calculated with Fourier coefficients ($|F_o| - |F_c|$) and phases calculated from the final model less the atoms of Tyr-143 and active-site solvent molecules. Refined atomic coordinates are superimposed on the map (contoured at 2.2σ); Val-121, Tyr-143, Thr-199, Trp-209, and zinc are indicated. The large six-membered ring of Tyr-143 essentially obliterates the pocket, and the "deep" water molecule (Lindskog, 1986) is displaced. The phenolic hydroxyl of Tyr-143 makes a long hydrogen bond interaction (within experimental error at 3.5 Å) with the non-protein zinc ligand; this ligand appears as an elongated electron cloud just above the zinc ion. Tyr-143 makes a 2.5-Å contact with another solvent molecule located near Val-121.

rings pack within the pocket. Neither the wild-type Val-143 side chain nor the phenylalanine and tyrosine mutant side chains exhibit optimal packing geometries as summarized by Ponder and Richards (1987). The conformation of the polypeptide backbone containing residue 143 does not exhibit much variation among the wild-type and mutant enzymes (Table II), so the hydrogen bond contacts defining the β-saddle (which includes residue 143) are not broken in V143F or V143Y CAIIs.

Intriguingly, the protein structure surrounding residue 143 appears to expand slightly in order to accommodate the large, partially buried side chains of Phe-143 and Tyr-143. Of course, the large aromatic side chains in V143F and V143Y CAIIs displace the "deep" water molecule in each structure (recall that this water resides at the mouth of the pocket in wild-type CAII). Furthermore, a weak hydrogen bond may exist between the phenolic hydroxyl of V143Y CAII and the non-protein zinc ligand with good stereochemistry [within experimental error: the O–O separation is 3.5 Å, the C–O–O angle is 124°, and the water is elevated by only 16° from the plane of the phenolic ring; see Thanki et al. (1988) and Ippolito et al. (1990)]. Although the refined position (at 2.8-Å resolution) of the non-protein zinc ligand in V143Y CAII is 4.0 Å away from zinc, the electron density corresponding to this ligand is fairly elongated and asymmetric (an inner-sphere binding mode might be modeled within this density; see Figure 2). The non-protein ligand in V143F CAII also appears elongated and asymmetric, such that two water molecules were modeled within the observed density (map not shown); the refined position (at 2.5-Å resolution) of the zinc-bound species is 2.1 Å away from zinc. If the non-protein zinc ligand is truly disordered in V143F and V143Y CAIIs, it may be that in one position it coordinates to the inner sphere of zinc and in the other position it hydrogen-bonds to the side chain of Tyr-143 in V143Y CAII.

The structure of V143Y CAII provides a mechanistic inference as to the structure of the CAII–phenol complex. Phenol is a competitive inhibitor of CAII-catalyzed CO_2 hydration and a noncompetitive inhibitor of bicarbonate dehydration, and it has been proposed that phenol binds in the hydrophobic pocket of native (i.e., wild-type) CAII without displacing zinc-bound hydroxide (Simonsson et al., 1982). As observed for the side chain of Tyr-143 in V143Y CAII, inhibitory phenol may bind in the hydrophobic pocket of wild-type CAII and donate a hydrogen bond to zinc-bound hydroxide, thereby occupying the substrate association site and also complexing/inactivating the catalytic nucleophile.

The three-dimensional structure of V143H CAII reveals that the five-membered ring of the imidazole side chain packs against the side of the hydrophobic pocket and, like the larger six-membered aromatic rings of V143F and V143Y CAII, tends toward an "edge-to-face" interaction (Burley & Petsko, 1988) with Trp-209. However, no classical hydrogen-bond contacts are observed for the imidazole side chain of His-143, so the conformational ambiguity characterizing χ_2 of this side chain cannot be resolved (i.e., carbon is indistinguishable from nitrogen in protein crystallographic experiments, so the distinction between χ_2 and $\chi_2 + 180°$ cannot be made). It is interesting to note that minor differences in side-chain torsion angles χ_1 and significant differences in χ_2 distinguish the packing of the six-membered aromatic rings in V143F and V143Y CAIIs from the five-membered imidazole ring in V143H CAII (χ_1 values differ by 4° and χ_2 values span a range of 25°; see Table II). Presumably, the smaller five-membered ring of the imidazole group can achieve an intimate packing arrangement within the confines of the hydrophobic pocket more easily than the larger six-membered aromatic rings. As found in V143F and V143Y CAIIs, however, side-chain torsion angles χ_1 and χ_2 (Table II) are not within the optimal ranges defined by Ponder and Richards (1987). Additionally, the torsion angles of the peptide units involving His-143 do not differ substantially from wild-type values (ϕ increases by 9° and ψ decreases by 9°; see Table II), so the β-sheet structure containing His-143 remains intact.

As observed in V143F and V143Y CAIIs, the protein structure surrounding His-143 in V143H CAII expands slightly in order to accommodate the large, partially buried imidazole side chain, and this side chain also displaces the "deep" water molecule observed in the wild-type enzyme at the mouth of the pocket. Although the electron density map of V143H CAII (Figure 3) is tantalizingly suggestive of a hydrogen-bond interaction between His-143 and the non-protein zinc ligand, the closest contact between the imidazole side chain and zinc-bound solvent is 3.8 Å. This distance is indicative of a weakly polar interaction, but it is too long to be considered a hydrogen bond. It is possible that this feature could be exploited in future experiments aimed at engineering the catalytic repertoire of the enzyme.

The crystal structure of the remaining mutant enzyme, V143G CAII, reveals that the lack of a large side chain at residue 143 results in some reorganization of the polypeptide backbone at this position; torsion angle ϕ increases by 22°,

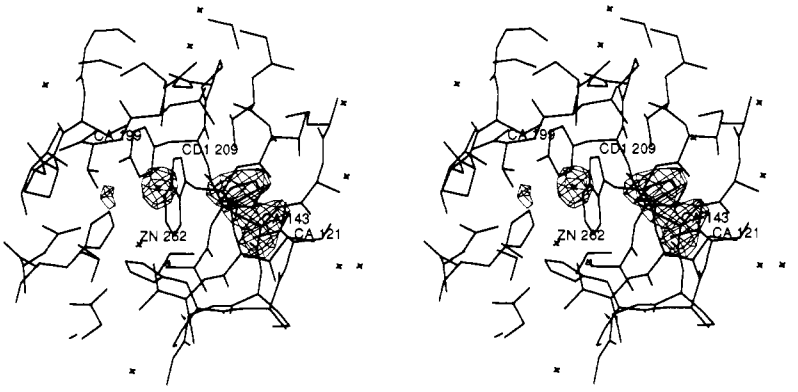

FIGURE 3: Difference electron density map of V143H CAII, calculated with Fourier coefficients ($|F_o| - |F_c|$) and phases calculated from the final model less the atoms of His-143 and active-site solvent molecules. The map is contoured at 3.1σ, and refined atomic coordinates are superimposed; Val-121, His-143, Thr-199, Trp-209, and zinc are indicated. Note that the side chain of His-143 appears to interact weakly with the non-protein zinc ligand, but this distance is too long (3.8 Å) to be considered a hydrogen bond.

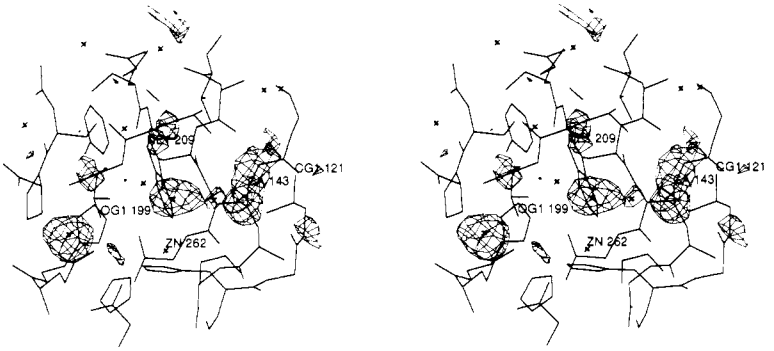

FIGURE 4: Difference electron density map of V143G CAII, calculated with Fourier coefficients ($|F_o| - |F_c|$) and phases calculated from the final model less the atoms of Gly-143 and active-site solvent molecules; the map is contoured at 2.5σ. Refined atomic coordinates are superimposed on the map, and Val-121, Gly-143, Thr-199, Trp-209, and zinc are indicated. Note that no significant electron density corresponding to the so-called "deep" water molecule (Lindskog, 1986) is observed; this water molecule is found at the mouth of the pocket in the wild-type enzyme.

and torsion angle ψ decreases by 14° relative to the wild-type enzyme (Table II; an electron density map of V143G CAII is found in Figure 4). These differences in backbone conformation are larger than those observed for the other mutants (V143H, V143F, and V143Y CAIIs) and probably reflect the greater flexibility conferred on the polypeptide backbone by substituting glycine for valine at position 143. However, hydrogen-bond interactions stabilizing the β-saddle containing Gly-143 are not broken. Although the Cα atom of residue 143 moves by 0.5 Å from its wild-type position toward the mouth of the hydrophobic pocket, the pocket is about 1 Å deeper than that of the wild-type enzyme, and the "walls" of the pocket (as defined by Val-121 and Trp-209) contract slightly.

Interestingly, no significant electron density is observed in the structure of V143G CAII that corresponds to the so-called "deep" water molecule (Lindskog, 1986) observed in the wild-type enzyme. This difference may arise from crystallographic differences characterizing V143G and wild-type CAIIs, e.g., crystal quality, number of reflections measured, etc. Since this water molecule is observed in the 2.4-Å resolution structure of Val-121 → Ala CAII [in this mutant, the hydrophobic pocket has a wider mouth; see Nair et al. (1991)], the moderate 2.4-Å resolution of the V143G CAII crystal structure is probably not a factor contributing to occupancy differences for the "deep" water molecule among wild-type, V121A, and V143G CAIIs.

The protein ligands comprising the zinc coordination polyhedra of all CAII mutants discussed above do not exhibit significant structural changes in response to mutations at residue 143, which is in reasonable proximity to the bound metal ion and its ligands (the Cα of Val-143 is 8.4 Å from Zn^{2+}). In general, the larger aromatic side chains of the V143Y and V143F mutants are within van der Waals distance of His-119, a zinc ligand. However, His-119 does not undergo substantial conformational changes in response to mutations at residue 143. We note that a possible compensatory movement of His-119 is seen in the 2.8-Å structure of V143Y CAII, but similar movements are not seen in V143F or V143H CAIIs; hence, the observed movement in V143Y CAII may be an artifact. Additionally, significant changes in histidine–zinc coordination distances are not apparent, with the exception of that involving His-96 in the V143G mutant, which lengthens by 0.4 Å (Table III).

Table III: Zinc–Ligand Distances[a] in Wild-Type and Mutant Carbonic Anhydrases II

ligand	wild type	V143Y	V143F	V143H	V143G
His-94	2.3	2.2	2.1	2.2	2.3
His-96	2.1	2.3	2.1	2.3	2.5
His-119	2.2	2.3	2.3	2.3	2.3
solvent	2.4	4.0	2.1	3.3	2.8

[a] Given in angstroms.

In contrast with the protein zinc ligands, significant differences in the coordination of the non-protein ligand to zinc are observed among the wild-type and mutant proteins. Zinc–ligand distances range from 2.1 to 4.0 Å (Table III), and electron density clouds corresponding to non-protein zinc ligands range from spherical and symmetric to elongated and asymmetric (Figures 2–4). Indeed, extreme values for this distance, such as the 4.0 Å observed in V143Y CAII, are not interpretable as inner-sphere metal interactions (in this ex-

ample, however, the corresponding electron density is elongated so that there is considerable "choice" for the optimal ligand position during crystallographic refinement—see Figure 2). To be sure, these phenomena may arise from crystallographic differences characterizing the structure determination of each protein. Alternatively, it is possible that the identity of the non-protein zinc ligand, which is presumed to be hydroxide ion, may be ambiguous under the conditions of crystallization. Both chloride ion and azide ion are present in the crystallization buffer at concentrations near their respective K_d values [Tibell et al. (1984) and Maren et al. (1976) and references cited therein]. Hence, it is conceivable that the non-protein zinc ligand observed in these crystal structures may actually be an equilibrium mixture of different anions; moreover, this equilibrium mixture may reapportion in response to different mutations at residue 143.

Discussion

Implications for Substrate Association. Spectroscopic studies of various metallosubstituted carbonic anhydrase isozymes from human or bovine sources suggest that enzyme–substrate association does not involve the inner-sphere interaction between a CO_2 oxygen and zinc (Riepe & Wang, 1968; Stein et al., 1977; Bertini et al., 1979, 1983, 1987; Led et al., 1982; Williams & Henkens, 1985). Instead, enzyme–substrate association displaces the so-called "deep" water molecule which binds at the mouth of the hydrophobic pocket in native CAII (Lindskog, 1986; Eriksson et al., 1986, 1988a); this water molecule is similarly displaced upon the binding of sulfonamide inhibitors (Eriksson et al., 1986, 1988b). Hence, the hydrophobic pocket may comprise the non-zinc substrate association site. Moreover, given that phenol is a competitive inhibitor of CO_2 hydration (Simonsson et al., 1982), and given the binding mode for phenol in the pocket inferred from the structure of V143Y CAII, the hydrophobic pocket is further implicated for the approach of the substrate toward nucleophilic zinc-bound hydroxide.

The measured kinetic behavior for each Val-143 mutant [Fierke et al., 1991 (preceding paper in this issue)] interpreted in view of the X-ray crystallographic results described herein are consistent with this proposal. Filling up the hydrophobic pocket by substituting a bulky side chain at the base, such as the five-membered ring imidazole side chain in V143H CAII, results in a 10^2-fold loss of activity relative to the wild-type enzyme; substituting the bulkier six-membered ring aromatic side chains of phenylalanine and tyrosine results in greater activity losses [V143F CAII, down by (5×10^4)-fold; V143Y CAII, down by (3×10^5)-fold]. Kinetic differences among V143H, V143F, and V143Y CAIIs may result from the different sizes of five- and six-membered rings, as well as the packing of these rings within the hydrophobic pocket: the imidazole side chain of His-143 packs differently in the pocket relative to the side chains of Phe-143 or Tyr-143 (Table II), such that the imidazole side chain does not fill up the pocket as much as the larger aromatic side chains (Figure 5).

Precatalytic binding modes of CO_2 in the hydrophobic pocket proposed by Merz (1990, 1991) and Liang and Lipscomb (1990) are qualitatively consistent with this structural and kinetic information. In Figure 5, the coordinates of CO_2 from a proposed CAII–CO_2 complex (Merz, 1990, 1991) are superimposed upon the coordinates of wild-type, V143H, and V143F CAIIs, and it is clear that CO_2 (or bicarbonate) association is less hindered in V143H CAII than in V143F or V143Y CAIIs. Therefore, the catalysis of CO_2 hydration is systematically compromised in this series of mutant CAIIs: the 100-fold loss of activity from wild-type CAII to V143H CAII results from steric inhibition of CO_2 association; the additional 500-fold loss of activity from V143H CAII to V143F CAII is due to more extensive blockage of the CO_2 association; and the further 6-fold loss of activity from V143F CAII to V143Y CAII may result from a weak hydrogen bond between Tyr-143 and nucleophilic zinc-bound hydroxide.

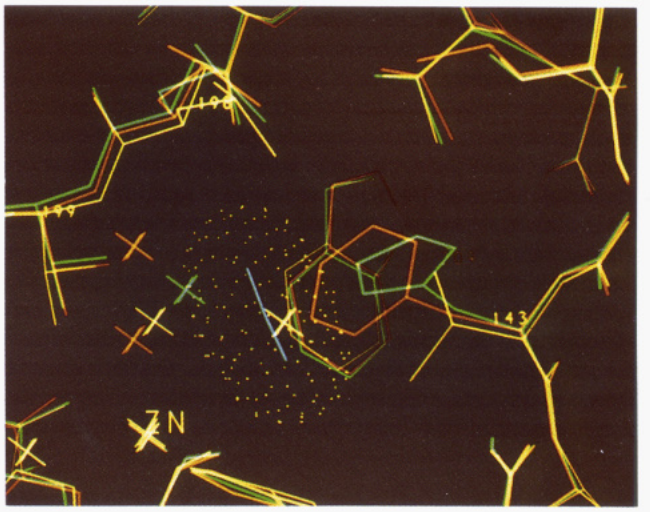

FIGURE 5: Coordinates of a proposed CO_2 binding mode (cyan, with van der Waals surface; Merz, 1990, 1991) superimposed on the structures of wild-type CAII (yellow), V143H CAII (green), and V143F CAII (red). Enzyme residues Val-143, Leu-198, Thr-199, and the active-site zinc ion are indicated. Note that the so-called "deep" water molecule (which appears as an unlabeled yellow star) at the mouth of the hydrophobic pocket in the wild-type enzyme must be displaced in order to accommodate CO_2; this water is also displaced by the mutated side chains of His-143, Phe-143, and Tyr-143 (Tyr-143 is not shown). Additionally, note that the calculated CO_2 binding mode is less hindered in V143H CAII (where CO_2 hydrase activity is diminished by 10^2-fold) than in V143F CAII [where CO_2 hydrase activity is diminished by (5×10^4)-fold]. Of course, the calculated CO_2 binding mode is not hindered in V143G CAII (structure not shown), which is consistent with the near-normal CO_2 hydrase activity measured for this particular mutant.

Since the V143G mutant exhibits near-normal CO_2 hydrase activity, it appears that as long as the pocket is as deep as, or deeper than, that of the wild-type enzyme, essentially normal activity results for residue 143 mutants; hence, the *volume* of the residue 143 side chain is critical for the activity of point mutants at this site [Fierke et al., 1991 (preceding paper in this issue)]. This complements structure–activity relationships among Val-121 mutants (Val-121 is at the mouth of the hydrophobic pocket), where the *hydrophobicity* of residue 121 is a significant feature characterizing the activity of point mutants (Nair et al., 1991). Given these data, it appears that the hydrophobic pocket of CAII is not required to define a unique precatalytic orientation of the substrate prior to catalysis, but it *is* required for substrate association. Given the symmetry of the CO_2 molecule and the resultant degrees of freedom for optimal nucleophilic attack, there is probably some latitude for acceptable substrate trajectories and orientations in the pocket that lead to efficient catalysis.

Compensatory Plasticity. In response to the mutation of even a single amino acid side chain, a protein structure may exhibit compensatory structural changes which accommodate the substitution. If the mutated side chain is on the surface of the protein, compensatory conformational changes of neighboring amino acids may be mediated by solvent [e.g., see Krebs et al. (1991)]. Alternatively, if the mutated side chain is buried or partially buried, compensatory structural changes may propagate through the protein scaffolding for some distance away from the point of mutation. These compensatory

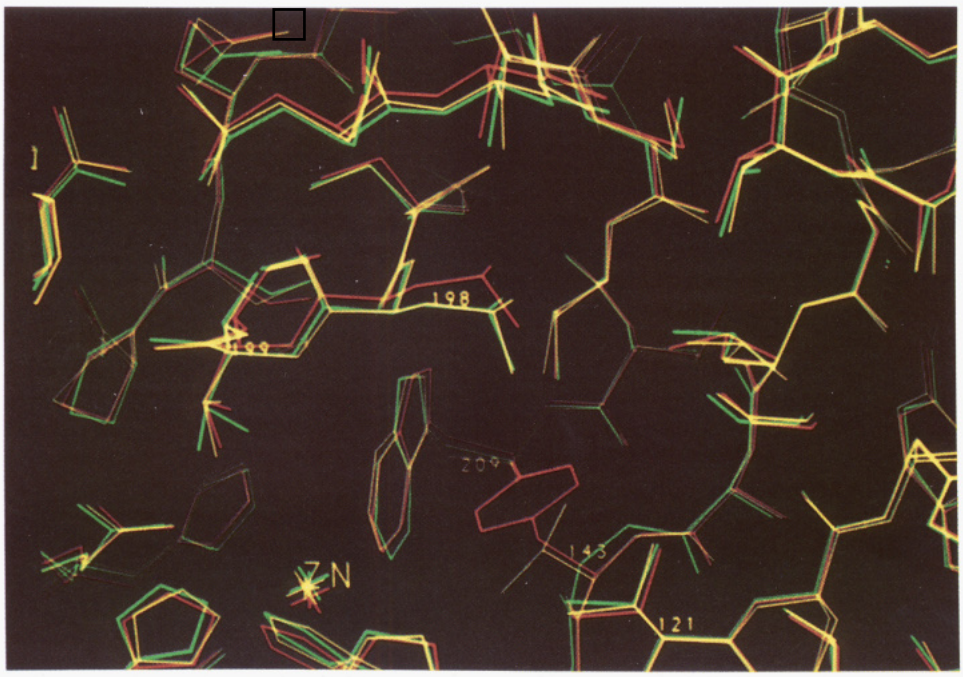

FIGURE 6: Superposition of wild-type CAII (yellow), V143Y CAII (red), and V143G CAII (green). Enzyme residues Val-121, Trp-209, Leu-198, Thr-199, and the active-site zinc ion are indicated. Note the compensatory expansion of the protein structure as the V143Y mutation is accommodated (similar expansions are observed in V143H and V143F CAIIs; structures are not shown); as expected, this expansion is not observed for V143G CAII (where, actually, a slight compensatory contraction of the hydrophobic pocket is observed in the movements of Trp-209 and Val-121). Some slight reorganization is evident for the peptide backbone of V143G CAII, and the Cα of Gly-143 moves toward the mouth of the pocket by about 0.5 Å.

changes generally involve slight readjustments of amino acid side chains which minimize small packing defects introduced by the mutation: this is a reflection of protein plasticity. Of course, a compromise must be attained between the optimization of packing interactions and the cost of strain energy incurred by movements away from optimal, equilibrium values for individual amino acid side chains (Ponder & Richards, 1987; Karpusas et al., 1989). Compensatory structural changes are expected to be greatest closest to the site of mutation (Perry et al., 1990), but it is conceivable that large segments of secondary structural elements will exhibit concerted structural changes in response to point mutations (segmental accommodation). However, α-helices are susceptible, whereas rigid β-sheets are not as susceptible, to such concerted reorganization (Perry et al., 1990; Eigenbrot et al., 1990).

Given our interest in (re)designing protein catalysts and their substrate recognition sites, e.g., specificity pockets, we acknowledge that the compensatory plasticity of a protein to amino acid substitutions must be fully characterized prior to rational protein design and engineering experiments. Here, CAII serves as a powerful example to illustrate the compensatory changes encountered as the result of redesigning the hydrophobic pocket. In CAII and in other systems, the mutation of partially buried amino acid side chains which define the contour of a pocket may result in subtle, compensatory contractions or expansions that propagate through a significant portion of the enzyme structure. Moreover, it is possible that compensatory structural effects could result in slight yet kinetically significant conformational changes of residues involved in catalysis, even if these residues are distant from the point of mutation. Structural analyses of wild-type CAII and the Val-143 variants herein reported yield the following hypothesis for amino acid substitutions at the base of the hydrophobic pocket: if a side chain larger than the wild-type side chain is substituted, a subtle, compensatory *expansion* results; if a side chain smaller than the wild-type side chain is substituted, a subtle, compensatory *contraction* results.

These compensatory changes are appreciable (on the order of 0.5–1.0 Å in the vicinity of the mutation); in spite of the differing resolutions of each mutant structure, the differences among the structures are real and significant [particularly given the typical rms coordinate errors of ca. 0.2 Å (Luzzati, 1952) and also the low thermal *B*-factors of relevant atoms (Bott & Frane, 1990)]. In Figure 6, the structures of wild-type, V143Y, and V143G CAIIs are superimposed to demonstrate the compensatory expansion (V143Y) and contraction (V143G) centered about residue 143. For instance, in V143Y CAII, where a bulky aromatic phenol group replaces the wild-type isopropyl group, a compensatory, concerted expansion of the protein scaffolding about the hydrophobic pocket is observed. The bulky Tyr-143 side chain causes the side chains of Leu-198 and Leu-141, which flank opposite sides of the pocket, to move away (Leu-198 moves by as much as 1 Å). In turn, the movement of Leu-198 propagates through to an adjacent region of the Ser-197–Cys-206 loop (which contains Leu-198); this loop connects two strands of the β-saddle. Importantly, catalytic residue Thr-199 is contained in this loop and undergoes minor structural changes in each mutant CAII, but it is difficult to estimate the impact of these changes on catalytic activity. Similar compensatory expansions are observed in the independently determined crystal structures of V143H and V143F CAIIs, so the assessment of a plastic response is not an artifact of a particular structure determined and refined at a particular resolution.

Although the structure of V143G CAII provides only one example of an amino acid substitution at residue 143 that results in a smaller side chain that that of the wild-type enzyme, there is nonetheless evidence of a compensatory, concerted contraction of the protein about the hydrophobic pocket. The isopropyl group of Val-143 buttresses the sides of the pocket in the wild-type enzyme; the loss of this buttressing

group in V143G CAII results in a slight, inward movement of Trp-209 (which comprises one side of the pocket; see Figure 6). Additionally, Val-121 (which is on the opposite side of the pocket from Trp-209) exhibits a slight inward movement. The net effect is a slight collapse of the walls and mouth of the hydrophobic pocket.

As for the β-saddle superstructure containing residue 143, there is no evidence for segmental accommodation of mutations at this position. Although minor differences in torsion angles ϕ and ψ are noted for residue 143 among wild-type and mutant CAIIs (Table II), these differences do not break the hydrogen-bond interactions defining the β-sheet. However, as noted above, propagated compensatory expansions result in appreciable structural changes to the Ser-197–Cys-206 loop region. This loop apparently acts as a "shock absorber" for the surrounding region of the β-saddle as large, partially buried mutations are accommodated at residue 143. Much smaller structural changes are observed in this loop region in the Val-121 → Ala mutant of CAII; like Val-143, Val-121 is part of the β-saddle but it is on an adjacent strand to that of Val-143, further away from the Ser-197–Cys-206 loop (Nair et al., 1991). Further protein design experiments will allow for the analysis of mechanisms by which amino acid mutations within β-sheet superstructures are accommodated—loop segments connecting the core β-strands may play a significant role as "shock absorbers" in the compensatory response to mutations.

The genetic–structural approach used to redesign the hydrophobic pocket of CAII is powerful, and such an approach is similarly successful in the engineering of specificity pockets in the serine proteases. For example, Bone et al. (1989) report that the Met-192 → Ala mutant of α-lytic protease exhibits nearly 10^6-fold greater activity toward substrates possessing P_1-Phe residues as compared with the wild-type enzyme (Met-192 is at the base of the S_1 pocket in the wild-type protease). X-ray crystallographic analysis of the mutant enzyme reveals a slight contraction of the pocket in response to the substitution of the smaller alanine for the larger methionine side chain at its base, and compensatory structural changes propagate for some distance away from the point mutation (Bone et al., 1989).

In work on another serine protease, the S_1 pocket of subtilisin has been redesigned by hydrophobic substitutions (Estell et al., 1986) and hydrophilic substitutions (Wells et al., 1987a) at the base of the pocket. X-ray crystal structure analyses of 20 subtilisin mutants reveal subtle and local perturbations about the point of mutation which result in kinetic differences in substrate binding and discrimination [Bott et al., 1987; Bott et al., unpublished work cited in Wells et al. (1987b)]. Importantly, Wells et al. (1987b) demonstrate that amino acid mutations beyond the direct enzyme–substrate contact region substantially affect substrate binding properties. This suggests that the plastic response of an enzyme structure accommodating individual or multiple point mutations may be exploited to enhance substrate binding and catalysis, even if such mutations are far removed from substrate binding or catalytic residues.

Summary and Conclusions

X-ray crystallographic studies of a series of CAII mutants, where mutations alter the contour of the hydrophobic pocket in the active site, allow for an assessment of the catalytic role of this pocket in light of the kinetics measured for each mutant [Fierke et al., 1991 (preceding paper in this issue)]. Mutations at Val-143, which is at the base of the pocket, result in significant changes in catalytic activity and protein structure. Differences in enzyme activity among six-membered ring aromatic groups and the five-membered ring imidazole group substituted for Val-143 arise from the different size and packing conformation for each side chain within the pocket. When glycine is substituted at this position, which results in a significantly deeper pocket, enzyme activity is only minimally altered. Structure–activity relationships for Val-121, at the mouth of the hydrophobic pocket, similarly indicate catalytic tolerance of mutations which alter the shape and character of the pocket (Nair et al., 1991). Hence, the hydrophobic pocket is important for substrate association with the enzyme and guides the substrate toward the catalytic nucleophile, but there are probably some number of catalytically acceptable substrate trajectories through this region of the enzyme structure that lead to efficient turnover.

Significant compensatory expansions or contractions of the protein around residue 143 are evident as the protein accommodates different side chains at this partially buried residue. Therefore, when a specificity pocket in any protein catalyst is redesigned, it is expected that compensatory and concerted conformational changes may propagate for appreciable distances (ca. 10–15 Å) away from amino acid mutations defining the base, walls, and mouth of the pocket. The average structure of this plastic response, as detected in X-ray crystallographic experiments, is not easily predictable from protein modeling studies utilizing simple graphics software. Furthermore, these effects might not be highlighted in rigorous modeling studies utilizing molecular dynamics methods since the compensatory structural changes accommodating point mutations are relatively small and on the scale of calculated thermal fluctuations (Karplus & Petsko, 1990). Nevertheless, the compensatory structural response of a protein structure to individual or multiple amino acid substitutions, as observed in CAII and other systems, must be well understood prior to the successful (re)design of effective protein catalysts.

Acknowledgments

We thank Dr. K. M. Merz for providing coordinates of the calculated CAII–CO_2 complex. We also thank Drs. J. E. Coleman, C. A. Fierke, K. M. Merz, J. Springer, B. McKeever, and A. Wei for helpful discussions.

Registry No. CAII, 9001-03-0; Val, 72-18-4.

References

Baldwin, J. J., Ponticello, G. S., Anderson, P. S., Christy, M. E., Murcko, M. A., Randall, W. C., Schwam, H., Sugrue, M. F., Springer, J. P., Gautheron, P., Grove, J., Mallorga, P., Viader, M.-P., McKeever, B. M., & Navia, M. A. (1989) *J. Med. Chem. 32*, 2510–2513.

Bernstein, F. C., Koetzle, T. F., Williams, G. J. B., Meyer, E. F., Brice, M. D., Rodgers, J. R., Kennard, O., Shimanouchi, T., & Tasumi, M. (1977) *J. Mol. Biol. 112*, 535–542.

Bertini, I., Borghi, E., & Luchinat, C. (1979) *J. Am. Chem. Soc. 101*, 7069–7071.

Bertini, I., Canti, G., & Luchinat, C., & Borghi, E. (1983) *J. Inorg. Biochem. 18*, 221–229.

Bertini, I., Luchinat, C., Monnanni, R., Roelens, S., & Moratal, J. M. (1987) *J. Am. Chem. Soc. 109*, 7855–7856.

Bone, R., Silen, J. L., & Agard, D. A. (1989) *Nature 339*, 191–195.

Bott, R., & Frane, J. (1990) *Protein Eng. 3*, 649–657.

Bott, R., Ultsch, M., Wells, J., Powers, D., Burdick, D., Struble, M., Burnier, J., Estell, D., Miller, J., Graycar, T., Adams, R., & Power, S. (1987) *Biotechnology in Agri-*

cultural Chemistry, ACS Symposium Series 334, pp 139–147, American Chemical Society, Washington, DC.
Burley, S. K., & Petsko, G. A. (1988) *Adv. Protein Chem. 39*, 125–189.
Christianson, D. W. (1991) *Adv. Protein Chem. 42*, 281–355.
Coleman, J. E. (1967) *J. Biol. Chem. 242*, 5212–5219.
Coleman, J. E. (1986) in *Zinc Enzymes* (Bertini, I., Luchinat, C., Maret, W., & Zeppezauer, M., Eds.) pp 49–58, Birkhauser, Boston.
Durbin, R. M., Burns, R., Moulai, J., Metcalf, P., Freymann, D., Blum, M., Anderson, J. E., Harrison, S. C., & Wiley, D. C. (1986) *Science 232*, 1127–1132.
Eigen, M., & Hammes, G. G. (1963) *Adv. Enzymol. Relat. Subj. Biochem. 25*, 1–38.
Eigenbrot, C., Randal, M., & Kossiakoff, A. A. (1990) *Protein Eng. 3*, 591–598.
Eriksson, A. E., Jones, T. A., & Liljas, A. (1986) in *Zinc Enzymes* (Bertini, I., Luchinat, C., Maret, W., & Zeppezauer, M., Eds.) pp 317–328, Birkhauser, Boston.
Eriksson, A. E., Jones, T. A., & Liljas, A. (1988a) *Proteins: Struct., Funct., Genet. 4*, 274–282.
Eriksson, A. E., Kylsten, P. M., Jones, T. A., & Liljas, A. (1988b) *Proteins: Struct., Funct., Genet. 4*, 283–293.
Estell, D. A., Graycar, T. P., Miller, J. V., Powers, D. B., Burnier, J. P., Ng, P. G., & Wells, J. A. (1986) *Science 233*, 659–663.
Fierke, C. A., Calderone, T. L., & Krebs, J. F. (1991) *Biochemistry* (preceding paper in this issue).
Forsman, C., Behravan, G., Jonsson, B.-H., Liang, Z.-W., Lindskog, S., Ren, X., Sandstrom, J., & Wallgren, K. (1988) *FEBS Lett. 229*, 360–362.
Henderson, L. E., Henriksson, D., & Nyman, P. O. (1976) *J. Biol. Chem. 251*, 5457–5463.
Hendrickson, W. A. (1985) *Methods Enzymol. 115*, 252–270.
Hendrickson, W. A., & Konnert, J. H. (1981) in *Biomolecular Structure, Conformation, Function and Evolution* (Srinivasan, R., Ed.). Vol. 1, pp 43–47, Pergamon, Oxford, England.
Ippolito, J. A., Alexander, R. S., & Christianson, D. W. (1990) *J. Mol. Biol. 215*, 457–471.
Jones, T. A. (1985) *Methods Enzymol. 115*, 157–171.
Jonsson, B.-H., Steiner, H. & Lindskog, S. (1976) *FEBS Lett. 64*, 310–314.
Karpusas, M., Baase, W. A., Matsumura, M., & Matthews, B. W. (1989) *Proc. Natl. Acad. Sci. U.S.A. 86*, 8237–8241.
Karplus, M., & Petsko, G. A. (1990) *Nature 347*, 631–639.
Krebs, J. F., Fierke, C. A., Alexander, R. S., & Christianson, D. W. (1991) *Biochemistry 30*, 9153–9160.
Led, J. L., Neesgaard, E., & Johansen, J. T. (1982) *FEBS Lett. 147*, 74–80.
Liang, J.-Y., & Lipscomb, W. N. (1988) *Biochemistry 27*, 8676–8682.
Liang, J.-Y., & Lipscomb, W. N. (1990) *Proc. Natl. Acad. Sci. U.S.A. 87*, 3675–3679.
Liljas, A., Kannan, K. K., Bergsten, P.-C., Waara, I., Fridborg, K., Strandberg, B., Carlbom, U., Jarup, L., Lovgren, S., & Petef, M. (1972) *Nature New Biol. 235*, 131–137.
Lindskog, S. (1983) in *Zinc Enzymes* (Spiro, T. G., Ed.) pp 78–121, Wiley, New York.
Lindskog, S. (1986) in *Zinc Enzymes* (Bertini, I., Luchinat, C., Maret, W., & Zeppezauer, M., Eds.) pp 307–316, Birkhauser, Boston.
Lindskog, S., & Coleman, J. E. (1973) *Proc. Natl. Acad. Sci. U.S.A. 70*, 2505–2508.
Luzzati, P. V. (1952) *Acta Crystallogr. 5*, 802–810.
Maren, T. H., Rayburn, C. S., & Liddell, N. E. (1976) *Science 191*, 469–472.
McPherson, A., Koszelak, S., Axelrod, H., Day, J., Williams, R., Robinson, L., McGrath, M., & Cascio, D. (1986) *J. Biol. Chem. 261*, 1969–1975.
Merz, K. M. (1990) *J. Mol. Biol. 214*, 799–802.
Merz, K. M. (1991) *J. Am. Chem. Soc. 113*, 406–411.
Nair, S. K., & Christianson, D. W. (1991) *J. Am. Chem. Soc.* (in press).
Nair, S. K., Calderone, T. L., Christianson, D. W., & Fierke, C. A. (1991) *J. Biol. Chem. 266*, 17320–17325.
Perry, K. M., Fauman, E. B., Finer-Moore, J. S., Montfort, W. R., Maley, G. F., Maley, F., & Stroud, R. M. (1990) *Proteins: Struct., Funct., Genet. 8*, 315–333.
Ponder, J. W., & Richards, F. M. (1987) *J. Mol. Biol. 193*, 775–791.
Riepe, M. E., & Wang, J. H. (1968) *J. Biol. Chem. 243*, 2779–2787.
Silverman, D. N., & Tu, C. K. (1975) *J. Am. Chem. Soc. 97*, 2263–2269.
Silverman, D. N., & Lindskog, S. (1988) *Acc. Chem. Res. 21*, 30–36.
Simonsson, I., Jonsson, B.-H., & Lindskog, S. (1982) *Biochem. Biophys. Res. Commun. 108*, 1406–1412.
Steigemann, W. (1974) Ph.D. thesis, Max-Planck-Institut fur Biochemie, 8033 Martinsried bei Munchen, FRG.
Stein, P. J., Merrill, S. P., & Henkens, R. W. (1977) *J. Am. Chem. Soc. 99*, 3194–3196.
Steiner, H., Jonsson, B.-H., & Lindskog, S. (1975) *Eur. J. Biochem. 59*, 253–259.
Ten Eyck, L. F. (1973) *Acta Crystallogr., Sect. A 29*, 183–191.
Ten Eyck, L. F. (1977) *Acta Crystallogr., Sect. A 33*, 486–492.
Thanki, N., Thornton, J. M., & Goodfellow, J. M. (1988) *J. Mol. Biol. 202*, 637–657.
Tibell, L., Forsman, C., Simonsson, I., & Lindskog, S. (1984) *Biochim. Biophys. Acta 789*, 302–310.
Tilander, B., Strandberg, B., & Fridborg, K. (1965) *J. Mol. Biol. 12*, 740–760.
Tu, C. K., Silverman, D. N., Forsman, C., Jonsson, B.-H., & Lindskog, S. (1989) *Biochemistry 28*, 7913–7918.
Wells, J. A., Powers, D. B., Bott, R. R., Graycar, T. P., & Estell, D. A. (1987a) *Proc. Natl. Acad. Sci. U.S.A. 84*, 1219–1223.
Wells, J. A., Cunningham, B. C., Graycar, T. P., & Estell, D. A. (1987b) *Proc. Natl. Acad. Sci. U.S.A. 84*, 5167–5171.
Williams, T. J., & Henkens, R. W. (1985) *Biochemistry 24*, 2459–2462.